LA-UR-06-3530

Approved for public release; distribution is unlimited.

Title: Recoil Products from p+118-Sn and d+118-Sn at 3.65 GeV/A

Author(s): A. R. Balabekyan, A. S. Danagulyan, J. R. Drnoyan, G. H. Hovhannisyan, N. A. Demekhina, J. Adam, V. G. Kalinnikov, M. I. Krivopustov, V. S. Pronskikh, V. I. Stegailov, A. A. Solnyshkin, P. Chaloun, V. M. Tsoupko-Sitnikov, S. G. Mashnik , and K. K. Gudima

Submitted to: Physics of Atomic Nuclei, 70 (2007) 1889;
E-print: nucl-ex/0603022

ISSN 1063-7788, Physics of Atomic Nuclei, 2007, Vol. 70, No. 11, pp. 1889–1897. © Pleiades Publishing, Ltd., 2007.

ELEMENTARY PARTICLES AND FIELDS
Experiment

Recoil Products from $p + {}^{118}$Sn and $d + {}^{118}$Sn at 3.65 GeV/A*

A. R. Balabekyan[1)**], A. S. Danagulyan[1)], J. R. Drnoyan[1)], G. H. Hovhannisyan[1)], N. A. Demekhina[2)], J. Adam[3),4)], V. G. Kalinnikov[3)], M. I. Krivopustov[3)], V. S. Pronskikh[3)], V. I. Stegailov[3)], A. A. Solnyshkin[3)], P. Chaloun[3),4)], V. M. Tsoupko-Sitnikov[3)], S. G. Mashnik[5)], and K. K. Gudima[6)]

Received December 5, 2006; in final form, April 12, 2007

Abstract—The recoil properties of the product nuclei from the interaction of 3.65-GeV/nucleon protons and deuterons from the Nuclotron and Synchrophasotron of the Laboratory of High Energies (LHE), Joint Institute for Nuclear Research (JINR) at Dubna, with a ^{118}Sn target have been studied using catcher foils. The experimental data were analyzed using the mathematical formalism of the standard two-step vector model. The analysis of kinematical characteristics of the light and medium-mass reaction products confirmed the contribution of fragmentation (or multifragmentation) processes in the production of these nuclei. The comparison of the results for protons and deuterons was made. The longitudinal momenta transferred to the target in the interaction with protons and deuterons were similar and was shown to depend only on the velocity, but not on the mass of projectile. Three different Los Alamos versions of the quark–gluon-string model (LAQGSM) were used for the discussion of our experimental results.

PACS numbers: 25.40.Vc, 24.10.-i
DOI: 10.1134/S1063778807110087

1. INTRODUCTION

In recent years, the interest in the recoil characteristics has been conditioned by the attempt to create a universal picture of interaction of high-energy projectiles with nuclei and determine the basic mechanism of development of nuclear reactions [1–6]. The possibility of a unified presentation of the momentum and energy distributions for target and projectile residuals enriches the whole picture and extends the models' conception.

The recoil properties of nuclei are often determined via "thick-target–thick-catcher" experiment using the induced activation method. In such experiments, the thicknesses of the target and catcher foils are larger than the longest recoil range. The quantities measured are the fractions F and B of product nuclei that recoil out of the target foil into the forward and backward directions, respectively.

The results of the experiment are usually processed by the standard two-step vector representation [7–9]. The following assumptions are made in this model:

In the first step, the incident particle interacts with the target nucleus to form an excited nucleus with velocity v, momentum p_{II}, and excitation energy E^*.

In the second step, the excited nucleus loses mass and excitation energy to form the final recoiling nucleus with an additional velocity V, which in general will have a distribution of values and directions.

Usually, additional assumptions are made in most experiments:

(i) The quantities v and p_{II} in the first step are constant [10] and lie in the forward direction.

(ii) The velocity in the second step is isotropic.

The results of the recoil experiments depend on the range–energy relation of the recoiling nuclei. It is convenient to express this relation as [8]

$$R = kV^n, \quad (1)$$

where R is the mean range (corresponding to V) of the recoil in the target material, and k and n are constants and can be evaluated from tables of ranges of nuclei recoiling into various materials [11]. The following relations are used for the forward and backward fractions:

$$FW = \frac{1}{4}R\left[1 + \frac{2}{3}(n+2)\eta + \frac{1}{4}(n+1)^2\eta^2\right], \quad (2)$$

*The text was submitted by the authors in English.

1)Yerevan State University, Yerevan, Armenia.
2)Yerevan Physics Institute, Armenia.
3)Joint Institute for Nuclear Research, Dubna, Russia.
4)INF AS, Řež, Czech Republic.
5)Los Alamos National Laboratory, Los Alamos, USA.
6)Institute of Applied Physics, Academy of Science of Moldova, Chişinău, Moldova.
**E-mail: balabekyan@ysu.am

$$BW = \frac{1}{4}R\left[1 - \frac{2}{3}(n+2)\eta + \frac{1}{4}(n+1)^2\eta^2\right],$$

where $\eta = v/V$ and W is the target thickness in mg/cm^2.

The reaction-product mean ranges (R) and the velocities transferred to residuals in the first (v) and second (V) steps of reaction are calculated using the following expressions [8]:

$$F/B = \frac{1 + \frac{2}{3}(n+2)\eta + \frac{1}{4}(n+1)^2\eta^2}{1 - \frac{2}{3}(n+2)\eta + \frac{1}{4}(n+1)^2\eta^2}; \quad (3)$$

$$R = 2W(F+B)/\left(1 + \frac{1}{4}(n+1)^2\eta^2\right).$$

The analysis of recoil properties in the wide range of initial energies and target (projectile) mass was made in many studies [1–6, 12]. The interpretation of the main regularities in the framework of the two-step model allows one to choose the spallation channel. Systematic deviations of the resulting parameters were attributed to the presence of fragmentation. The results of our previous investigations [13–15] showed that the cross sections of the light residuals at projectile energies up to several GeV are confirmed by the model calculations including the multifragmentation decay of the excited nuclei after cascade. The range of medium-mass products was partly involved in this process. For a more exact presentation of the production mechanism of medium-mass nuclei, measurements and analysis of the recoil properties in the reactions on ^{118}Sn with protons (3.65 GeV) and deuterons (7.2 GeV) are performed in the present work.

2. EXPERIMENTAL SETUP AND RESULTS

Targets of enriched tin isotope ^{118}Sn were irradiated at the Nuclotron and Synchrophasotron of the LHE, JINR, by proton and deuteron beams with energies of 3.65 GeV/nucleon. Irradiations were of 6.42 h for the proton beam and 1.083 h for the deuteron beam. The deuteron beam had an elliptic form with axes of 3 and 2 cm. The proton beam had circular form with a diameter of 2 cm. For beam monitoring, we employed the reactions ^{27}Al$(d, 3p2n)^{24}$Na, and ^{27}Al$(p, 3pn)^{24}$Na whose cross sections were taken as 14.2 ± 0.2 mb [16] and 10.6 ± 0.8 mb [17], respectively. From the monitoring reactions, the following beam intensities were obtained: 0.768×10^{13} d/h and 0.114×10^{13} p/h. The total beam fluences were 3.21×10^{13} protons and 2×10^{13} deuterons.

The target consisted of a high-purity target metal foil of size 20×20 mm sandwiched exactly between one pair of Mylar foils of the same size, which collected the recoil nuclei in the forward or backward directions with respect to the beam. The enrichment of the target was 98.7%, the thickness of each target foil was 66.7 mg/cm^2, and the number of target piles was 15. The whole stack, together with an Al beam-monitor foil of 140-mg/cm^2 thickness, was mounted on a target holder and irradiated in air.

After irradiation, the target foils and all the forward and backward catcher foils from one target pile were collected separately and assayed for radioactivities nondestructively with high-purity Ge detectors at LNP, JINR, for 1 yr. The radioactive nuclei were identified by characteristic γ lines and by their half-lives. The spectra were evaluated with the code package DEIMOS32 [18].

The kinematic characteristics of 30 product nuclei were obtained for deuteron- and proton-induced reactions. The relative quantities of the forward- and backward-emitted nuclei (relative to the beam direction) were calculated from the relations

$$F = N_F/(N_t + N_F + N_B); \quad (4)$$
$$B = N_B/(N_t + N_F + N_B),$$

where N_F, N_B, and N_t are the numbers of nuclei emitted in the forward and backward catchers and formed in the target foils, respectively. The recoil parameters obtained in these experiments are the forward-to-backward ratio, F/B, and the mean range, $2W(F+B)$. (The mean range of the recoils is somewhat smaller than $2W(F+B)$, but it is conventional to refer to the latter quantity as range.) The mathematical formalism of the standard two-step vector model [8] was used to process the experimental results. The parameters k and n in Eq. (1) are obtained by fitting the range dependence on energy of accelerated ions within the region from 0.025 to 5 MeV/nucleon [19]. It is possible to calculate η and v from Eq. (3), knowing the F/B ratio of the experiment.

Our experimental results are shown in Tables 1 and 2. We note that uncertainties concerning definite quantities in our tables are not listed to keep the tables concise. These uncertainties are about 10–15%.

As is shown in Fig. 1, the ratios F/B for both proton- and deuteron-induced reactions versus $\Delta A/A_t$ ($\Delta A = A_t - A_{\rm res}$, where A_t is the mass number of target and $A_{\rm res}$ is the mass number of product nuclei) are about 3 to 4 for heavy product nuclei and decrease to about 2 for light residuals.

Heavy residual nuclei are produced mainly via spallation mechanism, with products preferably in the forward direction. Light products have a more isotropic distribution in the target rest frame. Such

Table 1. Kinematic characteristics of product nuclei from deuteron-induced reactions

Product	F/B	η	$4W(F+B)$	T_{kin}, MeV	v, $(\text{MeV/amu})^{1/2}$	E^*, MeV
^{24}Na	2.03	0.175	4.08 ± 0.40	15.75 ± 2.37	0.2255	619.62
^{28}Mg	1.77	0.142	4.49 ± 0.70	19.70 ± 4.80	0.1913	527.36
^{42}K	2.36	0.212	2.49 ± 0.68	12.07 ± 5.11	0.1861	496.32
^{43}K	2.73	0.246	1.93 ± 0.35	7.54 ± 2.42	0.1680	449.30
^{44m}Sc	2.00	0.172	2.49 ± 0.58	12.21 ± 4.63	0.1457	394.77
^{52g}Mn	1.97	0.168	0.94 ± 0.21	2.86 ± 1.03	0.0678	172.55
^{56}Mn	2.39	0.215	1.67 ± 2.61	6.91 ± 4.06	0.1212	329.11
^{67}Ga	2.18	0.193	1.51 ± 7.44	6.89 ± 3.21	0.0996	270.13
^{73}Se	3.08	0.274	0.72 ± 0.66	2.25 ± 0.83	0.0769	210.08
^{75}Br	3.02	0.269	0.94 ± 0.28	3.46 ± 1.70	0.0927	252.67
^{77}Br	1.97	0.167	1.41 ± 0.39	6.51 ± 2.88	0.0785	212.61
^{81}Rb	4.09	0.338	1.14 ± 0.14	4.85 ± 0.98	0.1318	361.96
^{71}As	2.84	0.255	1.45 ± 0.27	6.74 ± 2.03	0.1261	343.88
^{83}Sr	3.39	0.296	1.11 ± 0.21	4.73 ± 1.45	0.1130	309.10
^{85}Y	3.51	0.304	0.89 ± 0.12	3.35 ± 0.72	0.0963	263.75
^{86m}Y	3.09	0.275	0.97 ± 0.13	3.88 ± 0.82	0.0934	254.93
^{87m}Y	3.44	0.299	0.97 ± 0.17	3.88 ± 1.12	0.1010	276.46
^{86}Zr	4.78	0.372	0.78 ± 0.11	2.78 ± 0.66	0.1061	292.67
^{89}Zr	2.96	0.265	0.88 ± 0.16	3.33 ± 0.97	0.0821	224.13
^{90}Mo	2.39	0.214	0.84 ± 0.17	3.26 ± 1.08	0.0657	178.49
^{93m}Mo	2.07	0.179	0.52 ± 0.07	1.46 ± 0.33	0.0362	98.25
^{90}Nb	3.28	0.288	0.45 ± 0.09	2.38 ± 0.48	0.0515	140.56
^{94}Tc	3.12	0.277	0.36 ± 0.09	0.86 ± 0.34	0.0423	115.53
^{95}Tc	3.82	0.323	0.54 ± 0.08	1.61 ± 0.39	0.0669	183.76
^{96}Tc	2.06	0.179	0.36 ± 0.06	0.85 ± 0.21	0.0270	73.29
^{97}Ru	3.64	0.312	0.66 ± 0.16	2.28 ± 0.89	0.0764	209.48
^{99m}Rh	3.56	0.307	0.45 ± 0.07	1.27 ± 0.33	0.0555	152.21
^{104}Ag	4.46	0.357	0.23 ± 0.05	0.45 ± 0.14	0.0332	103.03
^{109}In	3.24	0.286	0.26 ± 0.04	0.58 ± 0.14	0.0374	90.91

Table 2. Kinematic characteristics of product nuclei from proton-induced reactions

Product	F/B	η	$2W(F+B)$	T_{kin}, MeV	v, $(\text{MeV/amu})^{1/2}$	E^*, MeV
^{24}Na	1.95	0.165	5.37 ± 0.35	23.91 ± 2.36	0.2628	583.06
^{28}Mg	2.03	0.175	4.61 ± 0.30	20.54 ± 2.11	0.2399	530.01
^{42}K	2.15	0.189	3.12 ± 0.20	17.88 ± 2.04	0.2023	435.23
^{43}K	2.19	0.194	2.37 ± 0.14	10.83 ± 1.16	0.1595	343.19
^{44m}Sc	2.50	0.225	2.83 ± 0.18	14.97 ± 1.57	0.2111	463.51
^{46}Sc	1.94	0.165	2.94 ± 0.20	15.60 ± 1.68	0.1547	338.71
^{48}Sc	2.08	0.181	2.55 ± 0.34	12.07 ± 2.60	0.1467	321.13
^{48}V	2.21	0.196	2.56 ± 0.19	13.67 ± 1.67	0.1687	369.73
^{52g}Mn	2.21	0.196	2.09 ± 0.14	10.43 ± 1.09	0.1415	310.03
^{58}Co	3.21	0.284	2.38 ± 0.18	12.66 ± 1.54	0.2122	467.95
^{67}Ga	2.72	0.245	1.66 ± 0.11	8.04 ± 0.84	0.1362	299.48
^{71}As	3.83	0.324	1.54 ± 0.10	7.39 ± 0.79	0.1665	368.74
^{73}Se	3.96	0.331	0.97 ± 0.06	3.62 ± 0.37	0.1174	260.25
^{75}Se	5.17	0.389	0.98 ± 0.02	3.77 ± 0.15	0.1378	307.88
^{77}Br	3.23	0.285	0.94 ± 0.06	3.37 ± 0.35	0.0954	210.39
^{81}Rb	4.48	0.358	1.30 ± 0.07	5.99 ± 0.56	0.1547	344.22
^{82}Rb	3.68	0.314	0.73 ± 0.05	2.39 ± 0.25	0.0858	189.87
^{83}Sr	3.32	0.291	1.22 ± 0.08	5.51 ± 0.58	0.1199	264.95
^{85}Y	3.97	0.331	1.00 ± 0.07	3.99 ± 0.42	0.1143	253.54
^{86m}Y	4.7	0.369	1.21 ± 0.08	5.51 ± 0.58	0.1478	329.47
^{86}Zr	3.83	0.324	0.75 ± 0.05	4.88 ± 0.43	0.1179	272.26
^{89}Zr	3.82	0.323	1.04 ± 0.07	4.36 ± 0.46	0.1138	252.26
^{90}Mo	4.30	0.349	1.19 ± 0.08	5.74 ± 0.60	0.1401	311.45
^{90}Nb	4.03	0.335	0.70 ± 0.05	2.37 ± 0.25	0.0863	191.72
^{93m}Mo	3.74	0.318	0.68 ± 0.05	2.27 ± 0.25	0.0792	175.55
^{94}Tc	3.91	0.328	0.51 ± 0.03	1.49 ± 0.16	0.0656	145.55
^{95}Tc	3.59	0.309	0.65 ± 0.04	2.12 ± 0.22	0.0740	163.99
^{96}Tc	2.93	0.262	0.43 ± 0.04	1.12 ± 0.15	0.0453	100.00
^{97}Ru	3.86	0.326	0.53 ± 0.03	1.60 ± 0.17	0.0666	147.87
^{99m}Rh	4.23	0.346	0.43 ± 0.03	1.18 ± 0.12	0.0599	133.43
^{104}Ag	4.00	0.333	0.25 ± 0.02	0.50 ± 0.05	0.0369	81.99
^{109}In	3.94	0.330	0.22 ± 0.01	0.42 ± 0.04	0.0325	72.33

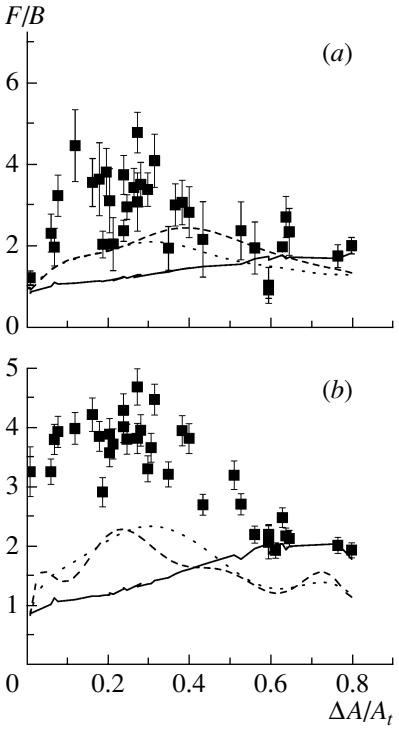

Fig. 1. F/B versus the fractional mass losses $\Delta A/A_t$: (a) for deuteron-induced reactions, (b) for proton-induced reactions. Curves show calculations (solid) by LAQGSM03.01, (dashed) by LAQGSM03.S1, and (dotted) by LAQGSM03.G1.

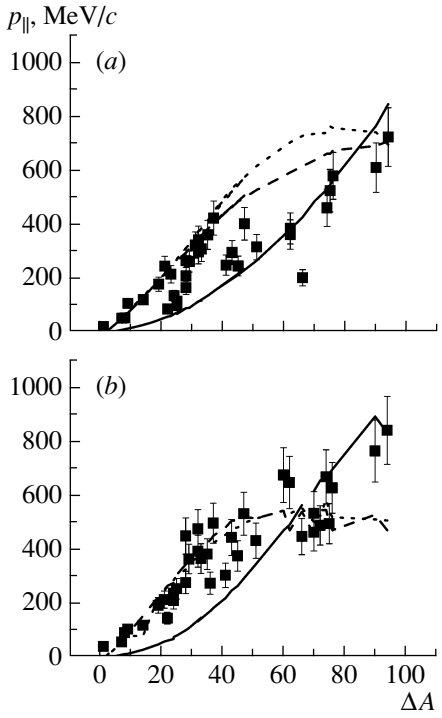

Fig. 2. Dependence of average longitudinal momentum on the number of emitted nucleons: (a) for deuteron-induced reactions, (b) for proton-induced reactions. Curves show calculations (solid) by LAQGSM03.01, (dashed) by LAQGSM03.S1, and (dotted) by LAQGSM03.G1.

a dependence could be explained by different mechanisms for the production of nuclei in different mass regions. In some early experiments at high energies [20], the authors referred to enhanced sideward emission of the light residuals followed by the decreasing F/B ratio. This effect leads to the manifestation of specific mechanisms in the production of light nuclei. Some of our recent studies [13–15] point to the multifragmentation mechanism in the formation of product nuclei with light and medium mass numbers.

As was shown from the comparison of the data in Tables 1 and 2, the average longitudinal velocity and momentum in the initial step of interaction obtained from our measurements in deuteron- and proton-induced reactions are approximately equal. It means that the transfer longitudinal momentum in the initial interaction is independent of the projectile mass. The fact of the dependence of this value on the projectile velocity or kinematical factor on the entrance channel was pointed out in [1]. A number of authors [21, 22] discussed the dependence of longitudinal momentum on projectile energy in units of projectile mass number. Our results of average longitudinal momentum (Fig. 2) for the evaporation products in reactions by proton and deuteron beams are 365 and 180 MeV/c per projectile nucleon, respectively. The comparison with the summary data [21, 22] shows that the investigated reactions run with the limiting value of transfer longitudinal momentum. Probably, protons are more effective agents of linear momentum transfer on a per-nucleon basis when compared with deuterons. On the whole, the tendency of increasing linear momentum on the nucleon loss is displayed in Fig. 2 in a common way [1]. After $\Delta A > 50$, it can be seen that the experimental points are deflected from the initial dependence.

The value of the forward velocity v may be used to determine the average cascade deposition energy (excitation energy E^*). The relation between the excitation energy and v may be estimated as [23]

$$E^* = 3.253 \times 10^{-2} k' A_t v [T_p/(T_p + 2)]^{0.5}, \quad (5)$$

where E^* and the bombarding energy T_p are expressed in terms of $m_p c^2$, A_t is the target mass in amu, and v is in units of $(\mathrm{MeV/amu})^{0.5}$. The constant k' has been evaluated by Porile on the basis of Monte Carlo cascade calculations as $k' = 0.8$ ([23] and references therein).

The evaluated "experimental" excitation energies of residual nuclei produced after the first, cascade,

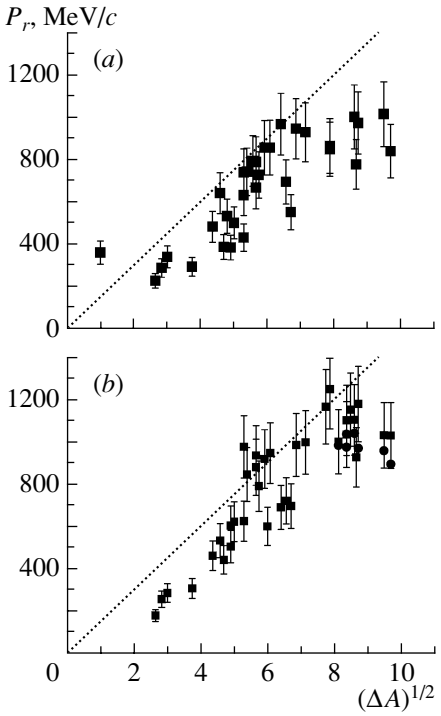

Fig. 3. The momentum of recoil nuclei as a function of observed mass loss: (*a*) for deuteron-induced reactions, (*b*) for proton-induced reactions. Dotted line is the systematics of Morrissey [1].

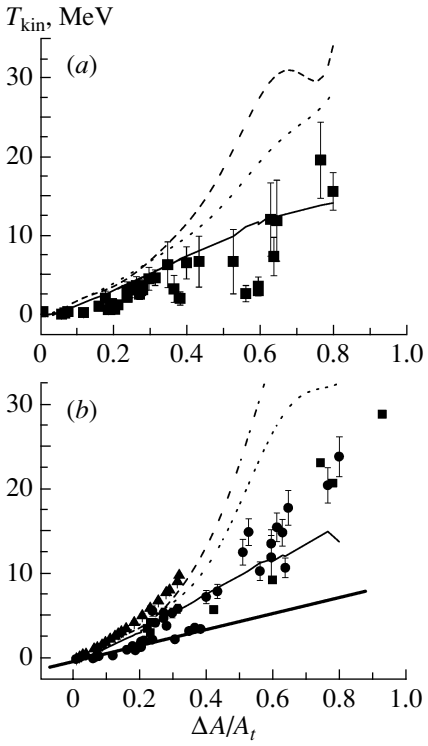

Fig. 4. Dependence of the kinetic energy of the product nuclei on the fractional mass losses $\Delta A/A_t$ (*a*) for (■) deuteron-induced reactions and (*b*) for (●) the proton-induced reactions. For comparison, the experimental results for (■) Ag target tabulated in [12] and for (▲) Pb target tabulated in [4] are presented in Fig. 4*b*. Curves show calculations (solid) by LAQGSM03.01, (dashed) by LAQGSM03.S1, and (dotted) by LAQGSM03.G1. Thick solid line is the linear fit of experimental data.

stage of reactions are shown in the last column of Tables 1 and 2.

As is seen from the tables, the excitation energies estimated according to Eq. (5) are higher than the multifragmentation threshold $E_{\text{th}} = 2$–4 MeV/nucleon ($E_{\text{tot}} = 216$–424 MeV) [24] for the light and medium products ($60 < \Delta A < 94$). This could be an indication that light and medium fragments are produced not only via the evaporation mechanism, but also via multifragmentation.

In Fig. 2, there is no comparison with the online measured longitudinal-momentum values [4–6] because of the absence of tabular data. However, the dependence of longitudinal momentum on spallation evaporation residues ([6], Fig. 10) is similar to ours.

The momentum of recoil nuclei (P_r) as a function of observed mass loss for the deuteron- and proton-induced reactions are shown in Fig. 3. In this figure, our data were compared with the systematics of Morrissey (dotted line) [1]. The slope of our experimental points was 150 MeV/c (similar to the Morrissey systematics) and corresponded to the average total kinetic energy of 12 MeV/nucleon.

Figure 4 shows the dependence of the fragment's kinetic energy T_{kin} on the fractional mass loss $\Delta A/A_t$. The kinetic energies of residuals increase practically linearly with the increase in $\Delta A/A_t$, but change their slope around $\Delta A/A_t \approx 0.5$. Cumming and Bächmann [25] and Winsberg [9] have shown that T_{kin} should increase linearly with $\Delta A/A_t$ for reactions in which the velocity of the product is due to the vectorial addition of the randomly directed recoil velocities resulting from particle emission. To compare, Fig. 4*b* shows also data measured for an Ag target by Porile et al. (see Table II in [12] and references therein) and for a Pb target tabulated in [4]. One can see that the Ag results agree well with our current ^{118}Sn data. For the Pb target, the dependence is similar to our results (considering the difference in energies and mass). For the higher $\Delta A/A_t$ in ^{208}Pb, the fission fragments should predominate over spallation and that is why experimental data are absent in Fig. 4*b*.

The value of the slope (Fig. 4) in the region of less emission nucleons ($\Delta A/A_t < 0.6$) is 12 MeV/nucleon (which corresponds to the value T_{kin} calculated from the slope of P_r) and obviously corresponds

to the evaporation mechanism of production at the average value of kinetic energy of emitting nucleons 12–15 MeV. The change in slope of a linear trend for our data up to 37 MeV/nucleon, seen in Fig. 4 for large fractional mass losses ($\Delta A/A_t \sim 0.6$), probably indicates a change in the spallation mechanism of the production of light nuclides.

The formation of light fragments from highly excited nuclei is of permanent interest in the literature and usually considers a multibody breakup [26]. One possible mechanism for such a process would be a simultaneous clustering of nucleons into fragments near the liquid–gas critical point [27]. This process is essentially different from the sequential evaporation process by which deep spallation products are formed. The comparison of our experimental results of T_{kin} with the calculations by three versions of LAQGSM models [29, 30] also manifests the contribution of multibody breakup [26]. Our experimental points for proton-induced reactions lie higher than the theoretical calculations by the cascade-evaporation mechanism (Fig. 4*b*). It appears that the kinetic energies of the products provide a qualitative method for distinguishing between these two mechanisms [28].

Our early comparison of the experimental cross sections with the available theoretical calculation by the LAHET, FLUKA, and LAQGSM agrees satisfactorily enough with LAQGSM calculation [15]. Therefore, in this paper, the recoil properties of residues are compared only with theoretical calculations by the several modifications of the LAQGSM model [29, 30].

LAQGSM03.01 [29] is the latest modification of the Los Alamos version of the quark–gluon string model (QGSM) [31], which in turn is an improvement of the QGSM [32]. It describes reactions induced by both particles and nuclei as a three-stage process: intranuclear cascade (INC), followed by preequilibrium emission of particles during the equilibration of the excited residual nuclei formed during the INC, followed by evaporation of particles from or fission of the compound nuclei. The INC stage of reactions is described with a recently improved version [29] of the time-dependent intranuclear cascade model developed initially at Dubna, often referred to in the literature simply as the Dubna intranuclear cascade model (see [33] and references therein). The preequilibrium part of reactions is described with an improved version [34] of the modified exciton model [35]. The evaporation and fission stages of reactions are calculated with an updated and improved version of the generalized evaporation model code GEM2 by Furihata [36], which considers evaporation of up to 66 types of different particles and light fragments (up to ^{28}Mg). If the excited residual nucleus produced after the INC has a mass number $A \leq 11$, LAQGSM03.01 uses a recently updated and improved version of the Fermi breakup model (in comparison with the version described in [32]) to calculate its decay instead of considering a preequilibrium stage followed by evaporation from compound nuclei, as described above. LAQGSM03.01 also considers coalescence of complex particles up to ^{4}He from energetic nucleons emitted during the INC, using an updated coalescence model in comparison with the version described in [33].

LAQGSM03.S1 [30] is exactly the same as LAQGSM03.01, but it also considers multifragmentation of excited nuclei produced after the preequilibrium stage of reactions, when their excitation energy is above $2A$ MeV, using the statistical multifragmentation model (SMM) by Bondorf et al. [27] (the "S" in the extension of LAQGSM03.S1 stands for SMM).

LAQGSM03.G1 [30] is exactly the same as LAQGSM03.01, but it uses the fission-like binary-decay model GEMINI of Charity et al. [37], which considers evaporation of all possible fragments, instead of using the GEM2 model [36] (the "G" stands for GEMINI).

In Figs. 1, 2, and 4, the theoretical calculations by the above models are presented.

As can be seen from Fig. 1, there is some disagreement between experimental data and theoretical results by all three versions of LAQGSM considered here. When making such a comparison, we first recognize that the experiment and the calculations differ in that (i) the experimental data were extracted assuming the "two-step vector model" [7–9], while the LAQGSM calculations were made without the assumptions of this model; and (ii) the measurements were performed on foils (thick targets), while the calculations were done for interactions of protons/deuterons with nuclei (thin targets). These differences must be considered before assessing possible deficiencies of the models. The behavior of initial interaction is expressed in the value and dependence of parameters of longitudinal velocity $v_{\|}$ and momentum $p_{\|}$ transferred in the initial step of reaction. The comparison with the model calculations permits us to assume that, for proton- and deuteron-induced reactions in the region $\Delta A \leq 40$, the LAQGSM03.S1 and LAQGSM03.G1 models possibly hold. In general, all the theoretical calculations do not explain experimental points in the whole region of mass loss.

As one can see from Fig. 4, the results by LAQGSM03.S1, which considers multifragmentation [27] of excited nuclei when their excitation energy is above 2 MeV/nucleon, overestimate significantly

the values of the measured mean kinetic energies of light products. This could be an indication that multifragmentation becomes important only at higher excitation energies, 4–5 MeV/nucleon instead of 2 MeV/nucleon as considered by LAQGSM03.S1, in complete agreement with the very recent ISIS measurements [38].

3. CONCLUSIONS

The new results of recoil properties in the reactions of ^{118}Sn with protons and deuterons of energy 3.65 GeV/nucleon are obtained.

The comparison of the data from deuteron- and proton-induced reactions confirms the independence of transferred longitudinal momentum in initial interaction of the projectile mass.

The comparison of transferred longitudinal momentum per nucleon confirms that, probably, protons are more effective agents of linear momentum transfer compared with deuterons.

The analysis of experimental results indicates the possible contribution of the multifragmentation mechanism in the production of light and medium-mass residuals.

ACKNOWLEDGMENTS

We would like to express our gratitude to the operating personnel of the JINR Nuclotron and Synchrophasotron for providing good beam parameters and to thank Dr. A.J. Sierk of LANL for a most useful critical reading.

This work was supported partially by the US DOE.

REFERENCES

1. D. J. Morrissey, Phys. Rev. C **39**, 460 (1989).
2. H. Haba, H. Matsumura, K. Sakamoto, et al., Radiochim. Acta **88**, 375 (2000).
3. A. A. Arakelyan, A. R. Balabekyan, A. S. Danagulyan, and A. G. Khudaverdyan, Nucl. Phys. A **534**, 535 (1991).
4. T. Enqvist, W. Wlazlo, P. Armbruster, et al., Nucl. Phys. A **686**, 481 (2001).
5. F. Rejmund, B. Mustapha, P. Armbruster, et al., Nucl. Phys. A **683**, 540 (2001).
6. J. Taieb, K. H. Schmidt, L. Tassan-Got, et al., Nucl. Phys. A **724**, 414 (2003).
7. N. Sugarman, M. Campos, and K. Wielgoz, Phys. Rev. **101**, 388 (1956).
8. L. Winsberg, Nucl. Instrum. Methods **150**, 465 (1978).
9. L. Winsberg, Phys. Rev. C **22**, 2116 (1980).
10. R. G. Kortelling, C. R. Toren, and E. K. Hyde, Phys. Rev. C **7**, 1611 (1973).
11. L. Winsberg, At. Data Nucl. Data Tables **20**, 389 (1977).
12. L. Winsberg, Phys. Rev. C **22**, 2123 (1980).
13. V. Aleksandryan, J. Adam, A. Balabekyan, et al., Nucl. Phys. A **674**, 539 (2000).
14. A. R. Balabekyan, A. S. Danagulyan, J. R. Drnoyan, et al., Nucl. Phys. A **735**, 267 (2004).
15. A. R. Balabekyan, A. S. Danagulyan, J. R. Drnoyan, et al., Phys. At. Nucl. **69**, 1485 (2006).
16. Ts. Damdinsuren, V. I. Iluschenko, P. Kozma, et al., Yad. Fiz. **52**, 330 (1990) [Sov. J. Nucl. Phys. **52**, 209 (1990)].
17. R. Michel, M. Gloris, H.-J. Lange, et al., Nucl. Instrum. Methods Phys. Res. B **103**, 183 (1995).
18. J. Frána, J. Radioanal. Nucl. Chem. **257**, 583 (2003).
19. L. C. Northcliffe and R. F. Schilling, Nucl. Data, Sect. A **7**, 233 (1970).
20. W. G. Lynch, Annu. Rev. Nucl. Part. Sci. **37**, 493 (1987).
21. F. Saint Laurent, M. Conjeaud, R. Dayras, et al., Phys. Lett. B **110**, 372 (1982); F. Saint-Laurent, M. Conjeaud, R. Dayras, et al., Nucl. Phys. A **422**, 307 (1984).
22. M. Bronikowski and N. T. Porile, Phys. Rev. C **44**, 1661 (1991).
23. O. Scheidemann and N. Porile, Phys. Rev. C **14**, 1534 (1976).
24. A. S. Botvina and I. N. Mishustin, nucl-th/0510081.
25. J. B. Cumming and K. Bächmann, Phys. Rev. C **6**, 1362 (1972).
26. A. S. Botvina and I. N. Mishustin, Phys. Lett. B **294**, 23 (1992).
27. J. P. Bondorf, A. S. Botvina, A. S. Iljinov, et al., Phys. Rep. **257**, 133 (1995).
28. C. F. Wang and N. T. Porile, Nucl. Phys. A **468**, 711 (1987).
29. S. G. Mashnik, K. K. Gudima, M. I. Baznat, et al., Report No. LA-UR-05-2686, LANL (Los Alamos, 2005).
30. S. G. Mashnik, K. K. Gudima, M. I. Baznat, et al., Report No. LA-UR-06-1764, LANL (Los Alamos, 2006).
31. K. K. Gudima, S. G. Mashnik, and A. J. Sierk, Report No. LA-UR-01-6804, LANL (Los Alamos, 2001); http://lib-www.lanl.gov/la-pubs/00818645.pdf

32. N. S. Amelin, K. K. Gudima, V. D. Toneev, Yad. Fiz. **51**, 512, 1730 (1990) [Sov. J. Nucl. Phys. **51**, 327, 1093 (1990)]; N. S. Amelin, K. K. Gudima, S. Yu. Sivoklokov, V. D. Toneev, Yad. Fiz. **52**, 272 (1990) [Sov. J. Nucl. Phys. **52**, 172 (1990)]; N. Amelin, CERN/IT/ASD Report CERN/IT/99/6 (Geneva, 1999); http://wwwinfo.cern.ch/asd/geant4/G4UsersDocuments/UsersGuides/PhysicsReferenceManual/html/PhysicsReferenceManual.html

33. V. D. Toneev and K. K. Gudima, Nucl. Phys. A **400**, 173c (1983).

34. S. G. Mashnik, K. K. Gudima, A. J. Sierk, et al., Report No. LA-UR-05-7321, LANL (Los Alamos, 2005); RSICC Code Package PSR-532, http://www-rsicc.ornl.gov/codes/psr/psr5/psr-532.html

35. K. K. Gudima, S. G. Mashnik, and V. D. Toneev, Nucl. Phys. A **401**, 329 (1983).

36. S. Furihata, Nucl. Instrum. Methods Phys. Res. B **171**, 252 (2000); PhD Thesis (Tohoku Univ., Tohoku, 2003).

37. R. J. Charity, M. A. McMahan, G. J. Wozniak, et al., Nucl. Phys. A **483**, 371 (1988).

38. V. E. Viola, K. Kwiatkowski, L. Beaulieu, et al., nucl-ex/0604012.